Boundary Value Problems
a SpringerOpen Journal

RESEARCH Open Access

# Analysis of the magneto-thermoelastic vibrations of rotating Euler–Bernoulli nanobeams using the nonlocal elasticity model

Ahmed E. Abouelregal[1*], Marin Marin[2*] and Sameh S. Askar[3]

*Correspondence:
ahabogal@gmail.com;
m.marin@unitbv.ro
[1]Department of Mathematics, Faculty of Science, Mansoura University, Mansoura 35516, Egypt
[2]Department of Mathematics and Computer Science, Transilvania University of Brasov, Brasov, Romania
Full list of author information is available at the end of the article

**Abstract**

This paper introduces size-dependent modeling and investigation of the transverse vibrational behavior of rotating thermoelastic nanobeams by means of nonlocal elasticity theory. In the formulation, a model of thermal conductivity with two-phase delays (DPL) was utilized. By incorporating the interactions between phonons and electrons, this model took into account microstructural influences. Also, we have employed the state-space approach and Laplace transform approach to solve the governing equations, which were developed in the context of the nonlocal Eringen model. The nanobeam material is subjected to a changeable temperature field produced by the graphene tape attached to the nanobeam and connected to an electrical source. In addition, the nanobeam material is fully encompassed by an axially applied magnetic field. It has been revealed how coefficients such as the rotational angular velocity of the nanobeam, nonlocal coefficient, voltage, electrical resistance, and applied magnetic field influence its behavior.

**Keywords:** Rotating nanobeams; Thermoelasticity DPL model; Electrical source; Graphene tape

## 1 Introduction

As nanofabrication technology has advanced, nano-electro-mechanical systems (NEMS) have become more valuable in a wide range of technical fields. Because of this, it is beneficial to investigate the mechanical performance of different NEMS parts [1] taking into account its use in nanoturbines, nanomotors, rotating nanoactuators, etc. Since the advent of nanotechnology, spinning beams have been integrated into more miniaturized and precise instruments. As rotary nanomotors with regulated ultrahigh speeds, these structures have been designed and investigated experimentally to show how mechanical rotations may be used to precisely modify the releasing rate of biochemicals on nanoparticles [2]. Because of its significance in rotary nanodevices and molecular motors, the unidirectional rotation of nanobeams has been represented as nanoblades in nanoturbines [3]. This has allowed researchers to examine the nanoscale water flow and the drag force on a rotating



Springer

nanoscale beam. Experimental analysis may provide a more precise answer; however, it is extremely difficult to standardize the lab conditions needed for every potential combination of tests, boundary conditions, environment, etc. [4].

Academics and engineers have shown great interest in spinning beam structures of various sizes in recent decades. In addition to their employment as rotors, blades, turbines, etc., rotating beams have also found application in other contexts [5, 6]. Researchers have examined the mechanical and physical properties of rotating beams, specifically their vibration patterns, utilizing experimental data, theoretical foundations, modal-based fatigue analysis, etc., so that these structures may be used suitably in a wide variety of systems. Ebrahimi et al. [7] studied the wave dispersion behavior of a spinning FGMs nanobeam using the nonlocal elasticity framework of Eringen. Through the use of the nonlocal theory of flexibility, Narendar and Gopalakrishnan [8] demonstrated the wave dispersion conduct of a spinning nanotube. Hoshina et al. [9] presented a method that can rotate nanoobjects and switch the direction in which they are rotating in both macroscopic and nanoscopic regions. Nan et al. [10] demonstrated a worldwide method for the out-of-plane rotation of various objects, including spherical symmetry and isotropic things, by use of an arbitrary low-energy laser. Within the nonlocal thermoelasticity concept framework, Abouelregal [11] et al. demonstrated the effect that heat transfer has on the dynamics of a spinning nanobeam. On the framework of the Euler–Bernoulli beam idea, the system of equations was constructed to accomplish this goal by employing extended conduction of heat, including phase delays. Using nonlocal and nonclassical continuous mechanics, Narendar [12] established a rotating single-walled nanotube (SWCNT) model by simulating it as an Euler–Bernoulli beam. Rahmani et al. [13] created a GNT and RBT-based vibrational analysis for 2D-FG spinning nanobeams with pore sizes. Further, the 2D-FG porous model and a unique hybrid approach utilizing long-range interatomic responses were created. Tho et al. [14] presented a research study of rotating beam constructs based on the existing literature, considering elementary geometrical defects and electrical and magnetic influence via higher-order shear deformation concepts that have not been thoroughly explored.

The point's state is defined as a function of strain at that point, but interatomic regions are ignored entirely in the traditional continuum theories. Due to the lack of a well-established scientific assumption that strain is a function of size, research on nanosystems based on these assumptions provides inaccurate findings. In the absence of solid scientific assumptions, research on nanosystems provides inaccurate conclusions due to the use of unrealistic assumptions. Because traditional continuum mechanics concepts are not good enough for figuring out how micro- and nanostructured materials behave mechanically, people have come up with revised elasticity models like the couple stress (CS) [15, 16], strain gradient (SG) [17], general nonlocal (GN) [18], and Eringen's nonlocal (EN) [19–21] concepts as a way to fix the problem. As Eringen's nonlocal elasticity concept [19–21] treats a point as reliant on the state of the complete body, it provides a powerful and accurate framework for investigating nanobeams. Eringen's hypothesis also takes into account the small-scale parameter, which is not inconsequential when compared to the size of the nanostructured materials.

Various models have been proposed to explain heat transfer in elastic bodies. One of the most famous models is the traditional parabolic diffusion model, which focuses on the Fourier equation for heat transfer. When applying this model to some problems, it is

expected that the increase in temperature and the vector of heat flux will occur through a volume of matter simultaneously. This means that applying a heat flux vector to a small portion of the material results in an infinite rate of heat diffusion throughout the medium [22]. This model is not good enough because transient flows often happen over very short periods. On length scales that are many orders of magnitude more considerable than micro, we can see that the thermal field has wave-like properties. The Cattaneo–Vernotte (CV) heat transfer model was independently published by Cattaneo [23] and Vernotte [24] in 1958. It involves a lag between the heat transfer rate and the temperature gradient. In contrast to the Fourier transport rule, which assumes immediate heat transmission, the CV concept does not consider this.

There have been modifications and extensions to the traditional thermoelastic concept to account for the peculiarities of modern thermal models, such as the use of a hyperbolic equation for heat transfer. The models put forth by Lord and Shulman (LS) [25], Green and Lindsay (GL) [26], and Green and Naghdi (GN) [27, 28] are a few examples of these models. Additionally, to get beyond the limitations of the Fourier law and the CV theory, Tzou [29–31] came up with the dual-phase-lag (DPL) model. This model is based on the time required to complete the reaction mechanisms at the micro- or nanoscale.

Blade-like structures that conduct rotational motions can be described as rotating beams and can be found in both large practical mechanical systems (such as helicopter blades, airplanes, and ship propellers) and nanoscale devices (such as microturbines). As a result, it is interesting to examine the mechanical response of rotating nanobeam assemblies. The results of the experimental analysis may be more accurate, but standardization of the lab conditions required for each test, including boundary conditions, surroundings, and so on, is extremely difficult. Because of this problem, structural analysis has come to rely on mathematical models.

It is a significant and tough endeavor to precisely predict and understand spinning nanobeams because of their essential function in numerous nanodevices. For this study, we modeled the thermal vibrational response of spinning nanobeams by means of the differential form of the nonlocal theory of elasticity [19–21]. This work employs the nonlocal Eringen framework to shed light on the size-dependent thermal excitation behavior of nanobeams, as there has been no previous systematic analysis of nanobeam rotation. Also, the impact of electric and magnetic and thermal fields on the thermomechanical behavior of nanospinning systems under Coriolis effects will be studied and highlighted using the thermoelasticity theory with phase delays (DPL). Maxwell's equations are utilized to compute the transverse Lorentz force that is produced by an external magnetic field. The numerical results give an analysis of how the behavior of rotating nanobeams is affected by small nonlocal parameters, the angular velocity of rotation, hub radius, and thermal effects. This research may contribute to a more in-depth understanding of rotating nanobeams' thermomechanical patterns and processes.

The developed framework was utilized to analyze the behavior of a thermoelastic rotating nanobeam that undergoes a temperature gradient induced by a sinusoidal heat source and a uniform axial magnetic field. Moreover, a graphene ribbon that is superimposed on the nanobeam and embedded in an electric source generates a variable temperature field. The Laplace transform procedure has been applied to convert the time domain of differential equations into a space domain, in which the system of equations can be solved and analytical solutions produced. It involves a numerical interpretation, allowing investiga-

tion of the effects of spin, a nonlocal thermoelasticity model, and a magnetic field on the performance of nanobeams. Next, we present graphical representations of the numerical data and provide an in-depth physics analysis and interpretation.

## 2 Thermal nonlocal mathematical modeling

Due to the overprediction of outcomes in local theory-based analyses of tiny sizes, taking the small-scale effect into account is essential for making accurate predictions of micro- and nanostructures. The nonlocal Eringen model is one of the most well-known formulations of continuity mechanics, and it accurately accounts for effects on smaller scales. This allows for the prediction of the behavior of substantial nanosized objects, as opposed to the many equations required by the conventional continuum mechanic concept. The nonlocal stress tensor, denoted by $\tau_{ij}$, can be represented as follows, according to Eringen's concept of nonlocal elasticity [19–21]:

$$\left[\tau_{ij}(\boldsymbol{r})\right]^{\text{nonlocal}} = \int_V \mathcal{K}\left(|\boldsymbol{r},\boldsymbol{r_0}|,\xi\right)\left[\sigma_{ij}\left(\boldsymbol{r}'\right)\right]^{\text{local}} \mathrm{d}\Omega(\boldsymbol{r_0}), \tag{1}$$

where $\sigma_{ij}$ is the conventional local stress tensor, which can be defined using the following formula:

$$\sigma_{ij}(\boldsymbol{r_0}) = 2\mu\varepsilon_{ij}(\boldsymbol{r_0}) + \left(\lambda\varepsilon_{kk}(\boldsymbol{r_0}) - \gamma\theta(\boldsymbol{r_0})\right)\delta_{ij}, \tag{2}$$

where $\boldsymbol{r_0}$ and $\boldsymbol{r}$ are adjacent places and the stress tensor $\varepsilon_{ij}$ at these two locations is represented by

$$2\varepsilon_{ij} = \frac{\partial u_i}{\partial x_j} + \frac{\partial u_j}{\partial x_i}. \tag{3}$$

In Eqs. (1)–(3), $\mathcal{K}(|\boldsymbol{r},\boldsymbol{r_0}|,\xi)$ is known as the kernel function or nonlocal modulus, Euclidean form of the distance (neighborhood distance) is denoted by the variable $|\boldsymbol{r}-\boldsymbol{r_0}|$, $\xi = e_0 a/l$ is a constant of the material that varies according to the internal and external characteristic lengths ($a$ and $l$), which is called the nonlocal scale coefficient, and the value of the parameter $e_0$ was found by experimentation. Also, $\theta = T - T_0$, $T_0$ is the environmental temperature and $\Omega$ represents the space that the body takes up. It is possible to express the Lamé elastic coefficients as $\lambda = \nu E/(1-2\nu)(1+\nu)$ and $\mu = E/(2+2\nu)$.

Since it was difficult to use the integral constitutive connection, Eringen [20] came up with the following solution:

$$\tau_{ij}(\boldsymbol{r}) - \xi^2\nabla^2\tau_{ij}(\boldsymbol{r}) = \sigma_{ij}(\boldsymbol{r_0}). \tag{4}$$

After plugging Eq. (2) into Eq. (4), the nonlocal constitutive equations that follow are obtained:

$$\sigma_{ij} - (e_0 a)^2\nabla^2\sigma_{ij} = \lambda\varepsilon_{kk}\delta_{ij} + 2\mu\varepsilon_{ij} - \gamma\theta\delta_{ij}. \tag{5}$$

For the case where $\theta = 0$, where no effect of temperature variation is present, we revert to the constitutive relation for nonlocal elasticity.

Tzou [29–31] came up with the idea of dual-phase-lag (DPL) heat conduction to account for the fact that heat can only spread at a specific rate. According to the prediction made using the classical Fourier heat transfer model, the thermal signal can travel at an infinitely high speed. The following is a mathematical representation of this:

$$\boldsymbol{q} + \tau_q \frac{\partial \boldsymbol{q}}{\partial t} + \frac{\tau_q^2}{2} \frac{\partial^2 \boldsymbol{q}}{\partial t^2} = -K\nabla\theta - K\tau_\theta \frac{\partial}{\partial t}(\nabla\theta), \tag{6}$$

where $\tau_q$ is the phase lag of the heat flux ($\boldsymbol{q}$) and $\tau_\theta$ is the phase lag of the temperature gradient ($\nabla\theta$). In addition to this, the equation for energy can be presented as

$$\rho C_E \frac{\partial \theta}{\partial t} + \gamma T_0 \frac{\partial e}{\partial t} = -\nabla \cdot \boldsymbol{q} + Q. \tag{7}$$

By removing the heat flux $\boldsymbol{q}$ from Eqs. (5) and (7), we can get the DPL heat transport equation, which is given as

$$\left(1 + \tau_q \frac{\partial}{\partial t} + \frac{\tau_q^2}{2} \frac{\partial^2}{\partial t^2}\right)\left[\rho C_e \frac{\partial \theta}{\partial t} + \gamma T_0 \frac{\partial e}{\partial t} - Q\right] = K\nabla^2\theta + K\tau_\theta \frac{\partial}{\partial t}\left(\nabla^2\theta\right). \tag{8}$$

When $\tau_\theta$ and $\tau_q$ are set equal to zero in Eq. (8), the traditional parabolic equation for heat transfer is produced. When $\tau_\theta$ equals 0 and $\tau_q$ is greater than 0, one derives the hyperbolic equation that describes a single-phase delay.

Nano- and micro-electromechanical systems (NEMS) and MEMS, nanodevices, bottom electronics, and nanostructured materials are just a few of the many fields where the magnetic field effect can be used. Recent years have seen an increase in research on the magnetic properties of nanobeams and how they function when exposed to a magnetic field.

The Maxwell equations in the differential form are presented as follows under the conventional electromagnetic theory [32, 33]:

$$\boldsymbol{J} = \nabla \times \boldsymbol{h}, \qquad \nabla \times \boldsymbol{E} = -\mu_0 \frac{\partial \boldsymbol{h}}{\partial t}, \qquad \boldsymbol{E} = -\mu_0 \left(\frac{\partial \boldsymbol{u}}{\partial t} \times \boldsymbol{H}\right), \tag{9}$$

$$\boldsymbol{h} = \nabla \times (\boldsymbol{u} \times \boldsymbol{H}), \qquad \nabla \cdot \boldsymbol{h} = 0. \tag{10}$$

Current density ($\boldsymbol{J}$), induced magnetic field ($\boldsymbol{h}$), and the strength of electric field ($\boldsymbol{E}$) are all variables in Eqs. (9) and (10). Also, $\boldsymbol{H}$ is the total magnetic field, and the magnetic field permeability is denoted by $\mu_0$.

## 3 Nonlocal rotating nanobeam Euler–Bernoulli problem

The studied thermoelastic nanobeam illustrated in graph 1 has these dimensions: length $L$, width $b$, and thickness $h$. The nanobeam is completely immersed in a longitudinal magnetic field and continuously heated by convection, which is presented as a rectified sine wave. We will proceed further with the assumption that the nanobeam rotates about an axis parallel to the $z$-axis with a constant angular velocity $\Omega$ at a suitable distance from its first end, as is shown in Fig. 1. In addition, we supposed that the rotating nanobeam was sufficiently thin. As a result, the beam theory was taken from Euler–Bernoulli as an illustration of the thermomechanical behavior of a nanobeam. Cartesian coordinates $(x, y, z)$

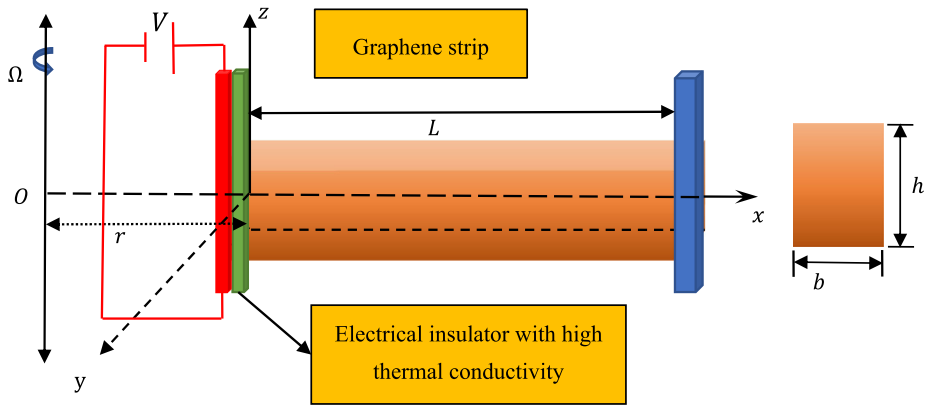


**Figure 1** A schematic representation of the revolving thermoelastic nanobeam

will be applied to study the proposed problem. Also, the graphene tape that is linked to the nanobeam and connected to an electrical source produces a variable temperature field, which is then applied to the material of the nanobeam. This causes the temperature of the field to change over time.

Based on the Euler–Bernoulli beam theory, which operates under the assumption of relatively minor deformations, the displacement components can be defined as

$$u_1 = u = -z\frac{\partial w}{\partial x}, \qquad u_2 = v = 0, \qquad u_3 = w = w(x,t), \tag{11}$$

where $w$ denotes the transversal displacement (deflection).

We take into account the axial initial magnetic field $\boldsymbol{H}$ as a vector that acts on the rotating nanobeam in the form of $\boldsymbol{H} = (H_0, 0, 0)$. In this particular instance, after applying Eqs. (8) and (9), the induced magnetic field $\boldsymbol{h}$ can be calculated as

$$\boldsymbol{h} = -H_x\left(\frac{\partial \boldsymbol{v}}{\partial y} + \frac{\partial \boldsymbol{w}}{\partial z}, -\frac{\partial \boldsymbol{v}}{\partial x}, -\frac{\partial \boldsymbol{w}}{\partial x}\right) = H_x\left(0, 0, \frac{\partial \boldsymbol{w}}{\partial x}\right). \tag{12}$$

When Eqs. (9) and (12) are used, the current density $\boldsymbol{J}$ is derived as

$$\boldsymbol{J} = \nabla \times \boldsymbol{h} = -H_x\left(0, \frac{\partial^2 w}{\partial x^2}, 0\right). \tag{13}$$

As a result, the Lorentz force $\boldsymbol{F}$ that is induced by the axial magnetic field that is being applied can be computed as

$$\boldsymbol{F} = (f_x, f_y, f_z) = \mu_0(\boldsymbol{J} \times \boldsymbol{H}) = \mu_0 H_x^2\left(0, 0, \frac{\partial^2 w}{\partial x^2}\right). \tag{14}$$

If this is the case, the magnetic force per unit length, also known as the resulting Lorentz force, will have the following form [34]:

$$f(x) = \int_A f_z \, \mathrm{d}A = A\mu_0 H_x^2 \frac{\partial^2 w}{\partial x^2}. \tag{15}$$

Because rotating parts are used so often in engineering, many researchers have been interested in how they behave mechanically. It has also been used to analyze the free vibrations of nanobeams, which rotate at varying speeds depending on their scale.

The centrifugal tension force $F_T(x)$ resulting from rotation appears when the nanobeam rotates around an axis parallel to the $z$-axis at a small distance from one of its ends with a constant angular velocity $\Omega$. The equation of motion for the nanobeam can now be derived by applying Hamilton's principle, considering the effect of the external forces acting on the nanobeam shown in the previous illustration. For rotating elastic Euler–Bernoulli beam, we have the following motion equations [35, 36]:

$$\frac{\partial^2 M}{\partial x^2} + f(x) = m\frac{\partial^2 w}{\partial t^2} - \frac{\partial}{\partial x}\left[F_T(x)\frac{\partial w}{\partial x}\right]. \tag{16}$$

The last component of Eq. (16) displays the impact of centrifugal force on the mechanical response of the structures, $m = \rho A$ represents the mass per unit length, $M$ is the bending moment, and $F_T(x)$ denotes the centrifugal force due to the rotation of the system.

The nonlocal constitutive relation provided in Eq. (5) for nanobeams takes the following form:

$$\sigma_x - \xi\frac{\partial^2 \sigma_x}{\partial x^2} = -E\left(z\frac{\partial^2 w}{\partial x^2} + \alpha_T\theta\right). \tag{17}$$

The moment of bending, denoted by $M$, can be represented as

$$M = \int z\sigma_x \,\mathrm{d}A. \tag{18}$$

With the help of relation (16), the moment can be obtained as a function of displacement by introducing Eq. (16) into Eq. (17) to get

$$M - \xi\frac{\partial^2 M}{\partial x^2} = -EI\left(\frac{\partial^2 w}{\partial x^2} + \alpha_T M_T\right). \tag{19}$$

The thermal bending moment, denoted by the symbol $M_T$, can be expressed in the form

$$M_T = \frac{12}{h^3}\int_{-h/2}^{h/2}\theta(x,z,t)z\,\mathrm{d}z. \tag{20}$$

We may extract the equation of motion for nonlocal Euler–Bernoulli beams by inserting $M$ from Eq. (18) into Eq. (15), which gives us the following:

$$\frac{\partial^4 w}{\partial x^4} + \frac{1}{EI}\left(1-\xi\frac{\partial^2}{\partial x^2}\right)\left(\rho A\frac{\partial^2 w}{\partial t^2} - A\mu_0 H_x^2\frac{\partial^2 w}{\partial x^2} - \frac{\partial}{\partial x}\left(F_T(x)\frac{\partial w}{\partial x}\right)\right) + \alpha_T\frac{\partial^2 M_T}{\partial x^2} = 0. \tag{21}$$

After ignoring the nonlocal scale factor $\xi$, this equation can be simplified to a classical version. At a certain distance $x$ from the origin $O$, the axial force $F_T(x)$ generated by the centrifugal stiffener can be expressed as follows:

$$F_T(x) = \int_x^L \rho A\Omega^2(r_{ad} + x)\,\mathrm{d}x. \tag{22}$$

The value of the constant $r_{ad}$ represents the incremental distance between the rotation axis and the beam's first side (hub radius). If Ω is equal to zero, then this indicates that there is no rotation, and as a result, the centrifugal tension force $F_T(x)$ is eliminated.

When the relationship (19) and the motion Eq. (16) are used together, the nonlocal bending moment $M$ may be written as

$$M = \rho A\xi \frac{\partial^2 w}{\partial t^2} - A\xi \mu_0 H_x^2 \frac{\partial^2 w}{\partial x^2} - \xi \frac{\partial}{\partial x}\left(F_T(x)\frac{\partial w}{\partial x}\right) - EI\left(\frac{\partial^2 w}{\partial x^2} + \alpha_T M_T\right). \tag{23}$$

The DPL heat transfer model for the current nanobeam can be stated as follows when the source of heat is not there ($Q = 0$):

$$\left(1 + \tau_q \frac{\partial}{\partial t} + \frac{\tau_q^2}{2}\frac{\partial^2}{\partial t^2}\right)\frac{\partial}{\partial t}\left[\rho C_e \theta - \gamma T_0 z \frac{\partial^2 w}{\partial x^2}\right] = K\nabla^2\theta + \tau_\theta K \frac{\partial}{\partial t}\left(\nabla^2\theta\right). \tag{24}$$

## 4 Solution procedure

Assume that with the increase in temperature $\theta$ the direction of the thickness of the nanobeam changes as a sinusoidal function in the variable $z$ as follows:

$$\theta(x,z,t) = \psi(x,t)\sin\left(\frac{\pi z}{h}\right). \tag{25}$$

When Eq. (25) is substituted into Eqs. (21) and (23), one obtains

$$EI\frac{\partial^4 w}{\partial x^4} + \left(1 - \xi\frac{\partial^2}{\partial x^2}\right)\left(\rho A\frac{\partial^2 w}{\partial t^2} - A\mu_0 H_x^2 \frac{\partial^2 w}{\partial x^2}\right) + \frac{24EI\alpha_T}{\pi^2 h}\frac{\partial^2 \psi}{\partial x^2} = (1 - \xi), \tag{26}$$

$$M = \rho A\xi \frac{\partial^2 w}{\partial t^2} - A\xi \mu_0 H_x^2 \frac{\partial^2 w}{\partial x^2} - \xi \frac{\partial}{\partial x}\left(F_T(x)\frac{\partial w}{\partial x}\right) - EI\left(\frac{\partial^2 w}{\partial x^2} + \frac{24T_0\alpha_T}{\pi^2 h}\psi\right). \tag{27}$$

In addition to this, the equation for heat conduction may be rewritten to take into account the size of the nanobeam, and it can then be represented as

$$\left(1 + \tau_q \frac{\partial}{\partial t} + \frac{\tau_q^2}{2}\frac{\partial^2}{\partial t^2}\right)\frac{\partial}{\partial t}\left[\frac{\rho C_E}{K}\psi - \frac{\gamma T_0 \pi^2 h}{24K}\frac{\partial^2 w}{\partial x^2}\right] = \left(1 + \tau_\theta \frac{\partial}{\partial t}\right)\left(\frac{\partial^2 \psi}{\partial x^2} - \frac{\pi^2}{h^2}\psi\right). \tag{28}$$

In the present investigation, the most significant axial force that can be exerted on a nanobeam due to the uniform rotation has been taken into account. The maximum axial force $F_T(x)$ due to centrifugal stiffening, in this case, can be written as follows [8, 37, 38]:

$$F_T(x) = F_{\max} = \int_0^L \rho A\Omega^2(r + x)\,\mathrm{d}x = \frac{1}{2}\rho A\Omega^2 L(2r + L). \tag{29}$$

Because of this, we can write the system of equations down as a partial differential equation with a constant parameter. The controlling mathematical formula for the transverse deformation $w(x,t)$ of a spinning microbeam is then found to be

$$\begin{aligned} &EI\frac{\partial^4 w}{\partial x^4} + \rho A\left(1 - \xi\frac{\partial^2}{\partial x^2}\right)\frac{\partial^2 w}{\partial t^2} - \left(A\mu_0 H_x^2 + F_{\max}\right)\left(1 - \xi\frac{\partial^2}{\partial x^2}\right)\frac{\partial^2 w}{\partial x^2} \\ &\quad = -\frac{24EI\alpha_T}{\pi^2 h}\frac{\partial^2 \psi}{\partial x^2}, \end{aligned} \tag{30}$$

$$M = \rho A\xi \frac{\partial^2 w}{\partial t^2} - \xi \left(A\mu_0 H_x^2 + F_{\max}\right)\frac{\partial^2 w}{\partial x^2} - EI\left(\frac{\partial^2 w}{\partial x^2} + \frac{24T_0\alpha_T}{\pi^2 h}\psi\right). \tag{31}$$

Variables in basic equations can be transformed by using the following nondimensional quantities:

$$\begin{aligned}
&\left\{u', w', x', z'\right\} = \frac{\vartheta_0}{k}\{u, w, x, z\}, \qquad \left\{t', \tau_q', \tau_\theta'\right\} = \frac{\vartheta_0^2}{k}\{t, \tau_\theta, \tau_\theta\},\\
&\xi' = \frac{\vartheta_0^2}{k^2}\xi, \qquad \psi' = \frac{\psi}{T_0}, \qquad \left\{L', h', b', r'\right\} = \frac{\vartheta_0}{k}\{L, h, b, r\},\\
&M' = \frac{k}{\vartheta_0 EI}M, \qquad k = \frac{K}{\rho C_E}, \qquad \vartheta_0^2 = \frac{E}{\rho}.
\end{aligned} \tag{32}$$

So, it is possible to write the nondimensional versions of the expressions for heat transfer, the motion equation, and the bending moment in simpler ways by omitting the primes, as shown here:

$$\frac{\partial^4 w}{\partial x^4} + \frac{12}{h^2}\left(1 - \xi\frac{\partial^2}{\partial x^2}\right)\frac{\partial^2 w}{\partial t^2} - \frac{12}{h^2}\left(a_0^2 + \frac{F_{\max}}{\rho A}\right)\left(1 - \xi\frac{\partial^2}{\partial x^2}\right)\frac{\partial^2 w}{\partial x^2} = -\frac{24\alpha_T}{\pi^2 h}\frac{\partial^2 \psi}{\partial x^2}, \tag{33}$$

$$M = \frac{12\xi}{h^2}\frac{\partial^2 w}{\partial t^2} - \frac{12\xi}{h^2}\left(a_0^2 + \frac{F_{\max}}{\rho A}\right)\frac{\partial^2 w}{\partial x^2} - \frac{\partial^2 w}{\partial x^2} - \frac{24T_0\alpha_T}{\pi^2 h}\psi, \tag{34}$$

$$\left(\frac{\partial}{\partial t} + \tau_q\frac{\partial^2}{\partial t^2} + \frac{\tau_q^2}{2}\frac{\partial^3}{\partial t^3}\right)\left[\psi - \frac{\gamma\pi^2 h}{24\eta K}\frac{\partial^2 w}{\partial x^2}\right] = \left(1 + \tau_\theta\frac{\partial}{\partial t}\right)\left(\frac{\partial^2 \psi}{\partial x^2} - \frac{\pi^2}{h^2}\psi\right), \tag{35}$$

where $a_0^2 = \frac{\mu_0 H_x^2}{\rho}$.

It is necessary to consider the initial and boundary conditions before attempting to solve the governing equations. Initially, the initial constraints can be assumed to be

$$w(x,0) = 0 = \frac{\partial w(x,0)}{\partial t}, \qquad u(x,0) = 0 = \frac{\partial u(x,0)}{\partial t}, \qquad \psi(x,0) = 0 = \frac{\partial \psi(x,0)}{\partial t}. \tag{36}$$

## 5 Solution in the transformed domain

Equations (33) and (34) are both partial differential equations of the fourth order, representing the equations of motion and heat transfer, respectively. Solving these differential equations mathematically and obtaining direct analytical results is a very challenging task due to its complex nature. In this context, the Laplace transform method converts them into ordinary equations for deflection and temperature change. When the Laplace transform is applied, the equations of system (33)–(35) can be rewritten as

$$A_0\frac{\mathrm{d}^4\overline{w}}{\mathrm{d}x^4} - A_1 s^2\frac{\mathrm{d}^2\overline{w}}{\mathrm{d}x^2} + A_2 s^2\overline{w} = -A_3\frac{\mathrm{d}^2\overline{\psi}}{\mathrm{d}x^2}, \tag{37}$$

$$-A_5\frac{\mathrm{d}^2\overline{w}}{\mathrm{d}x^2} = \frac{\mathrm{d}^2\overline{\psi}}{\mathrm{d}x^2} - A_4\overline{\psi}, \tag{38}$$

$$\overline{M} = -A_0\frac{\mathrm{d}^2\overline{w}}{\mathrm{d}x^2} + A_6\overline{w} - A_3\overline{\psi}, \tag{39}$$

where

$$A_0 = 1 + \frac{12\xi}{h^2}\left(a_0^2 + \frac{F_{\max}}{\rho A}\right), \qquad A_1 = \frac{12}{h^2}\left(a_0^2 + \frac{F_{\max}}{\rho A} + \xi s^2\right),$$
$$A_4 = \frac{\pi^2}{h^2} + \frac{1}{q}, \qquad A_2 = \frac{12s^2}{h^2}, \qquad A_3 = \frac{24T_0\alpha_T}{\pi^2 h}, \tag{40}$$
$$q = \frac{1 + \tau_\theta s}{s(1 + \tau_q s + s^2\tau_q^2/2)}, \qquad A_5 = \frac{\gamma c^2\pi^2 h}{24qK_0}, \qquad A_6 = \frac{12\xi s^2}{h^2}.$$

## 6 State-space approach technique

To use the state-space approach technique [39, 40] to solve the problem, we will present the function $\overline{\phi}$ defined using the relation

$$\frac{\mathrm{d}^2\overline{w}}{\mathrm{d}x^2} = \overline{\phi}. \tag{41}$$

When Eq. (41) is plugged into Eqs. (37) and (38), one arrives at the following result:

$$\frac{\mathrm{d}^2\overline{\phi}}{\mathrm{d}x^2} = -B_3\overline{w} - B_4\overline{\psi} + B_5\overline{\phi}, \tag{42}$$
$$\frac{\mathrm{d}^2\overline{\psi}}{\mathrm{d}x^2} = B_1\overline{\psi} - B_2\overline{\phi}, \tag{43}$$

where

$$B_1 = A_4, \qquad B_2 = A_5, \qquad B_3 = A_2 s^2, \qquad B_4 = \frac{A_3}{A_0}, \qquad B_5 = \frac{A_1 s^2}{A_0}. \tag{44}$$

In this part, we will attempt to find a solution to the existing issue by employing the direct integration approach by matrix exponential. Taking into consideration the following functions as being state variables

$$\overline{V}_1 = \overline{w}, \qquad \overline{V}_2 = \overline{\psi}, \qquad \overline{V}_3 = \overline{\phi},$$
$$\overline{V}_4 = \frac{\mathrm{d}\overline{V}_1}{\mathrm{d}x}, \qquad \overline{V}_5 = \frac{\mathrm{d}\overline{V}_2}{\mathrm{d}x}, \qquad \overline{V}_6 = \frac{\mathrm{d}\overline{V}_3}{\mathrm{d}x}, \tag{45}$$

it is possible to write Eqs. (41)–(43) in the form of a matrix as

$$\frac{\mathrm{d}\overline{V}(x,s)}{\mathrm{d}x} = \overline{V}'(x,s) = A(s)\overline{V}(x,s), \tag{46}$$

where

$$\overline{V}(x,s) = \begin{Bmatrix} \overline{V}_1 \\ \overline{V}_2 \\ \overline{V}_3 \\ \overline{V}_4 \\ \overline{V}_5 \\ \overline{V}_6 \end{Bmatrix}, \qquad A(s) = \begin{bmatrix} 0 & 0 & 0 & 1 & 0 & 0 \\ 0 & 0 & 0 & 0 & 1 & 0 \\ 0 & 0 & 0 & 0 & 0 & 1 \\ 0 & 0 & 1 & 0 & 0 & 0 \\ 0 & B_1 & -B_2 & 0 & 0 & 0 \\ -B_3 & -B_4 & B_5 & 0 & 0 & 0 \end{bmatrix}. \tag{47}$$

In the transform domain, the state vector is denoted by $\overline{V}(x,s)$, and its components are the temperature $\overline{\psi}$ and the deflection $\overline{w}$ after they have been changed, along with the gradients of those two variables.

System of Eqs. (46) is capable of being integrated with the help of the matrix exponential, which will result in

$$\overline{V}(x,s) = e^{A(s)x}\overline{V}(0,s). \tag{48}$$

The matrix $e^{\mathrm{A(s)}x}$ denotes the exponential transfer matrix, and $\overline{V}(0,s)$ is given by

$$\overline{V}(0,s) = \left\{\overline{w}, \overline{\psi}, \overline{\phi}, \frac{\mathrm{d}\overline{w}}{\mathrm{d}x}, \frac{\mathrm{d}\overline{\psi}}{\mathrm{d}x}, \frac{\mathrm{d}\overline{\phi}}{\mathrm{d}x}\right\}^{\mathrm{tr}}(0,s). \tag{49}$$

To determine the structure of the matrix denoted by the expression $e^{\mathrm{A(s)}x}$, we will make use of the well-established Cayley–Hamilton principle. For our novel state-space method, the square matrix $A(s)$ is analyzed to find the eigenvalues and eigenvectors $Y(x,s)$ that fulfill

$$A(s)Y(x,s) = \hbar Y(x,s). \tag{50}$$

This equation gives the characteristic solution for the matrix $A(s)$ as

$$\left|A(s) - \hbar I\right| = 0, \tag{51}$$

where $I$ is the identity matrix, $\hbar$ is a symbol for a particular root of $A(s)$, which allows the equation to be satisfied

$$\hbar^6 - l\hbar^4 + m\hbar^2 - n = 0, \tag{52}$$

where

$$l = B_1 + B_5, \qquad m = B_1B_5 - B_2B_4 + B_3, \qquad n = B_1B_3. \tag{53}$$

To solve the characteristic equation in matrix form, it is necessary to consider the Caley–Hamilton principle [41, 42]. According to the Hamilton theorem, the matrix $A(s)$ meets its own characteristic equation when viewed from a matrix perspective. Because of this, one can deduce that

$$\left[A(s)\right]^6 - l\left[A(s)\right]^4 + m\left[A(s)\right]^2 - n = 0. \tag{54}$$

It is possible to formulate the Taylor expansion of the transfer matrix $e^{A(s)x}$ as follows:

$$e^{A(s)x} = \sum_{n=0}^{\infty} \frac{[A(s)x]^n}{n!}. \tag{55}$$

This infinite series (55) can be simplified using the Cayley–Hamilton theorem, as shown below [41, 42]

$$e^{A(s)x} = a_0I + a_1A + a_2A^2 + a_3A^3 + a_4A^4 + a_5A^5 = \ell(x,s), \tag{56}$$

where the unknown parameters $a_j(x,s)$ are based on the values of $x$ and $s$. According to the Cayley–Hamilton theorem, the characteristic roots $\pm k_i$ ($i = 1, 2, 3$) of the matrix $A(s)$ are required to have equations that they satisfy, which means that

$$e^{\pm k_i x} = a_0 I + a_1 k_i + a_2 k_i^2 + a_3 k_i^3 + a_4 k_i^4 + a_5 k_i^5, \quad i = 1, 2, 3. \tag{57}$$

Appendix A illustrates the process of solving the equations presented above to obtain the parameters $a_j(x,s)$. As a result, the exponential matrix can be found by using the expression

$$e^{A(s)x} = \ell(x,s) = \left[\ell_{ij}(x,s)\right], \quad i,j = 1, 2, \ldots, 6, \tag{58}$$

where Appendix B provides the elements $\ell_{ij}(x,s)$.

## 7 Application and boundary conditions

It is known that an additional form of energy is released in the form of heat when an electric current flows through a conductive material. The amount of heat produced by an electric current depends on several factors, including the magnitude of the current, the resistance of the conductor, and the duration of the current flow. In the present problem, it is considered that an electric current, e.g., a voltage, passes through the graphene tape located at the first end of the nanobeam, as shown in Fig. 1. The thermal effect generated by the graphene tape connected to a voltage source allows the generated external heat to be transmitted and leads to heat flowing into the beam, according to Joule's theory of electric heating. According to Joule's first rule, the ability of an electrical conductor to generate heat is proportional to the amount of energy it can supply to an external resistance. In this case, we have the following relationship:

$$P = I_e^2 R_e, \tag{59}$$

where $I_e$ represents the amount of current passing through the resistor and $R_e$ represents the electrical resistance in the circuit. Ohm's law, $V_e = I_e R_e$, may be used as an input for the universal power calculation [43]

$$P = \frac{V_e^2}{R_e}, \tag{60}$$

where $V_e^2$ denotes the voltage.

It is necessary to assume that 100% of the applied energy is transformed into heat to determine the amount of heat energy produced by electrical resistance. The quantity of heat produced by the current flow is proportional to the length of the flow when the resistance and the current are kept constant. In this case, we will assume that the nanobeam is thermally loaded at its initial end ($x = 0$), which gives [44]

$$\psi(0,t) = I_e^2 R_e t = \frac{V_e^2}{R_e} t. \tag{61}$$

To accommodate various applications, various boundary conditions are employed. In this situation, we use the following sets of mechanical boundary conditions:

$$w(x,t)|_{x=0,L} = 0, \qquad \left.\frac{\partial^2 w(x,t)}{\partial x^2}\right|_{x=0,L} = 0. \tag{62}$$

In the Laplace transform domain, we can now transform Eqs. (61) and (62), respectively, as follows:

$$\overline{w}(x,s)|_{x=0} = 0, \qquad \left.\frac{\mathrm{d}^2\overline{w}(x,s)}{\mathrm{d}x^2}\right|_{x=0} = 0, \qquad \overline{\phi}(x,s)|_{x=0} = 0, \tag{63}$$

$$\overline{\psi}(x,s)|_{x=0} = \frac{V_e^2}{sR_e} = \overline{G}(s). \tag{64}$$

Also, we can impose the following conditions at the other end ($x = L$) of the nanobeam

$$\overline{w}(L,s) = \overline{\psi}(L,s) = \overline{\phi}(L,s) = 0. \tag{65}$$

Consequently, the values $\frac{\mathrm{d}\overline{w}(0,s)}{\mathrm{d}x}$, $\frac{\mathrm{d}\overline{\psi}(0,s)}{\mathrm{d}x}$, and $\frac{\mathrm{d}\overline{\phi}(0,s)}{\mathrm{d}x}$ may be written as

$$\frac{\mathrm{d}}{\mathrm{d}x}\begin{Bmatrix}\overline{w}\\ \overline{\psi}\\ \overline{\phi}\end{Bmatrix}(0,s) = -\overline{G}(s)\begin{bmatrix}\ell_{14}(L,s) & \ell_{15}(L,s) & \ell_{16}(L,s)\\ \ell_{24}(L,s) & \ell_{25}(L,s) & \ell_{26}(L,s)\\ \ell_{34}(L,s) & \ell_{35}(L,s) & \ell_{36}(L,s)\end{bmatrix}^{-1}\begin{Bmatrix}\ell_{12}(L,s)\\ \ell_{22}(L,s)\\ \ell_{32}(L,s)\end{Bmatrix}. \tag{66}$$

After applying several simplifications, one can arrive at the ultimate solutions to the functions $\overline{w}(x,s)$ and $\overline{\theta}(x,z,s)$ in the Laplace transform domain as follows:

$$\begin{aligned}\overline{w}(x,s) = \mathcal{S}\Bigg[&\frac{\sinh(k_1(L-x))}{(k_1^2-k_2^2)(k_1^2-k_3^2)\sinh(k_1L)} + \frac{\sinh(k_2(L-x))}{(k_2^2-k_1^2)(k_2^2-k_3^2)\sinh(k_2L)}\\ &+ \frac{\sinh(k_3(L-x))}{(k_3^2-k_2^2)(k_3^2-k_1^2)\sinh(k_3L)}\Bigg],\end{aligned} \tag{67}$$

$$\begin{aligned}\overline{\theta}(x,z,s) = -B_2\mathcal{S}\sin\left(\frac{\pi z}{h}\right)\Bigg[&\frac{k_1^2\sinh(k_1(L-x))}{(k_1^2-B_1)(k_1^2-k_2^2)(k_1^2-k_3^2)\sinh(k_1L)}\\ &+ \frac{k_2^2\sinh(k_2(L-x))}{(k_2^2-B_1)(k_2^2-k_1^2)(k_2^2-k_3^2)\sinh(k_2L)}\\ &+ \frac{k_3^2\sinh(k_3(L-x))}{(k_3^2-B_1)(k_3^2-k_2^2)(k_3^2-k_1^2)\sinh(k_3L)}\Bigg],\end{aligned} \tag{68}$$

where

$$\mathcal{S} = \frac{G(s)(B_1-k_1^2)(B_1-k_2^2)(B_1-k_3^2)}{B_1B_2}.$$

Using the previously derived formulas for $\overline{w}(x,s)$ and $\overline{\theta}(x,s)$, we can calculate the bending moment and the axial displacement $\overline{M}(x,s)$ and $\overline{u}(x,s)$.

## 8 Numerical inversion of the transformed functions

In straightforward situations, the inverse transform can be determined analytically or with the aid of tables. Evaluating the complex integration of the inverse transformation also yields the Laplace transform. Sometimes it is tough to spot the inverts. Possible explanations include the fact that the inverse is not a named function and hence cannot be expressed in a "simple" formula. Moreover, the issue is well posed only if the Laplace transform is neither calculable nor measured on the real and positive axes. For instance, the same transform applies to pairs of time-domain functions that differ at a single instant in time. The lack of a precise inversion formula makes this instance exceedingly challenging. In such circumstances, the adoption of a numerical approach is required. Numerous numerical algorithms have been published, each with its own set of uses and strengths when applied to specific classes of functions.

The Fourier series expansion technique will be briefly described here. The key to this approach is the integration of the contour Bromwich inversion, which can be written as the integral of a real-valued function of a real variable given a given contour. The inversion integral is turned into a Fourier transform, and then the Fourier transform is approximated by a Fourier series with a known error estimate (using the trapezoidal method). By using this method, we may convert any Laplace domain function into a time domain function by [45]

$$g(t) = \frac{e^{\mathcal{A}/2}}{t} Re\left[\overline{g}\left(\frac{\mathcal{A}}{2t}\right)\right] + \frac{e^{\mathcal{A}/2}}{t} Re\left[\sum_{\mathbb{K}=1}^{n_0} \overline{g}\left(\frac{\mathcal{A} + 2i\mathbb{K}\pi}{2t}\right)(-1)^{\mathbb{K}}\right]. \tag{69}$$

It is now possible to numerically calculate Eq. (69) by summing over a limited number of $\mathbb{K}$. The accuracy may be improved by adjusting the values of $\mathcal{A}$ and $\mathbb{K}$. Using this approach proves to be quite precise. Many computer tests have shown that the value of A must meet the relation $\mathcal{A} \cong 10$ [46] for convergence to happen faster.

## 9 Numerical results and discussions

Under the effect of a longitudinal magnetic field and a thermoelectric field, the thermal and mechanical wave scattering characteristics of immersed nanobeams will be examined, and a discussion will follow based on the formulae that were found using the nonlocal Euler—Bernoulli beam theory. In order to represent the patterns of the studied fields, including the temperature change, deformation, lateral vibration, and flexure moment, figures in the $x$ direction that are analyzed in terms of $x$, $z$, and $t$ can be utilized. Single-crystal silicon was selected as the material of choice so that numerical assessments could be performed. The following illustrates the problem's constants [47]:

$$E = 169\ \text{GPa}, \qquad \rho = 2330\frac{\text{kg}}{\text{m}^3}, \qquad \text{G} = 79.6\ \text{GPa}, \qquad C_E = 713\text{J/(kgK)},$$
$$T_0 = 317\text{K}, \qquad \alpha_T = 2.59 \times 10^{-6}(1/\text{K}), \qquad \nu = 0.064, \qquad K_0 = 156\text{W/(mK)}.$$

The calculations are performed using fixed aspect ratios for the rotating nano width, which is assumed to be 50 nm, $L/h = 10$, and $b/h = 0.5$. In addition to this, the values of the parameters $t = 0.12$ and $z = h/6$ are held constant. According to the definition given by Eringen [21], $e_0$ is a material-specific constant. For example, by comparing the network

dynamics results with those of the nonlocal concept, it was discovered that the value of $e_0$ for a given class of materials is equal to 0.39 [32]. According to Sudak [48], the $e_0$ values should be obtained from experimental data, although not many of them are available for nanobeams. The following are the three distinct categories that can be used in the discussions of results and numerical data.

According to the research that has been done so far, there has not been a complete analysis of the vibration aspects of spinning thermoelastic nanobeams. Considering the modified thermoelasticity theory in the formulation and incorporating the influence of the Joule theory of electric heating on the behavior of different research fields throughout the whole structure are both important considerations. Therefore, this study explores this topic to fill the gap that was revealed in the open literature related to the thermomechanical vibration of spinning nanobeams.

In this section, we will examine the influences of varying the rotational angular speed $\Omega$ on a rotating nanobeam in a homogeneous magnetic field and experiencing convection due to an electric current created in a graphene slab. It is supposed that the nonlocal coefficient, the electrical voltage, electrical resistance, and the phase delays are all constants in this scenario ($\xi = 0.3$, $Ve = 10$ V, $Re = 300$, $\tau_q = 0.05$, and $\tau_\theta = 0.02$). When there is no rotation, the angular speed of rotation is considered zero ($\Omega = 0$), which is treated as a particular case in this work. The fluctuation of the considered variables is depicted in Figs. 2 through 5 for four distinct values of angular speed $\Omega = 0$, 0.1, 0.3, and 0.4, respectively.

It is evident from Fig. 2 that the thermal deflection $w$ satisfies the suggested boundary condition of the problem as it vanishes at the two ends of the beam at $x = 0$ and $x = L$. It is also detected that as the angular velocity of rotation rises, the absolute value of the deflection decreases. As a result of the presence of the thermal source resulting from the electric current to which the beam is exposed, the accurate beam will have the highest absolute values towards the first side and decrease in the direction of the axial axis. Another thing to note about this diagram is that the deflection rapidly decreases from zero to its minimum value at point $x \cong 0.12$ and gradually decreases back to zero. There is a high degree of consistency between these results and those reported in [49].

Figure 3 shows that for different angular speeds of rotation $\Omega$, the temperature $\theta$ of the nanobeam is found to change with increasing distance $x$. The temperature profile $\theta$ expands slightly as the spin speed increases. Moreover, it is seen that the temperature curves

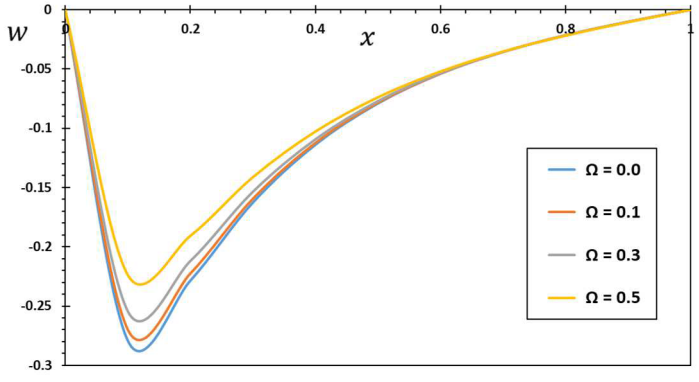


**Figure 2** The effect of rotation ($\Omega$) on the variation of deflection $w$

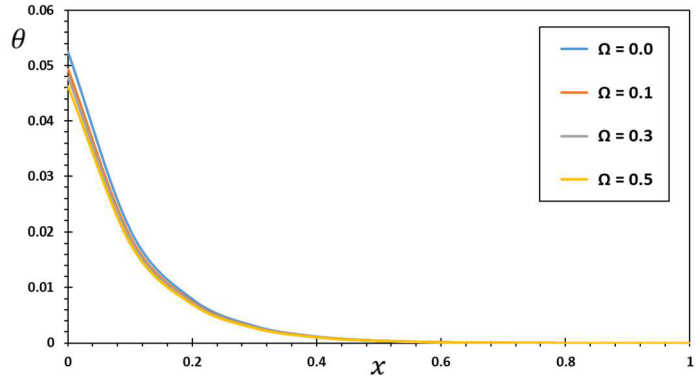


**Figure 3** The effect of rotation (Ω) on the variation of temperature $\theta$

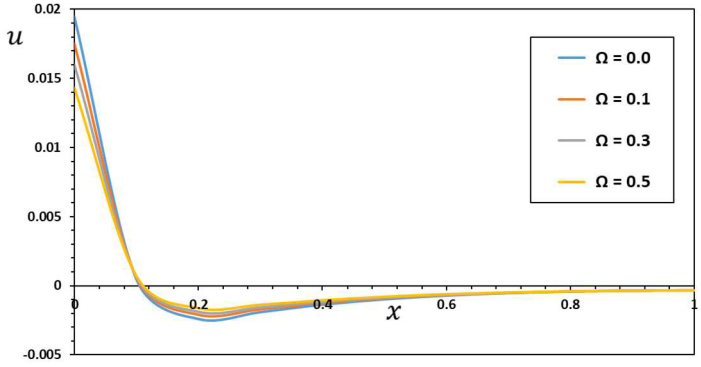


**Figure 4** The effect of rotation (Ω) on the variation of displacement $u$

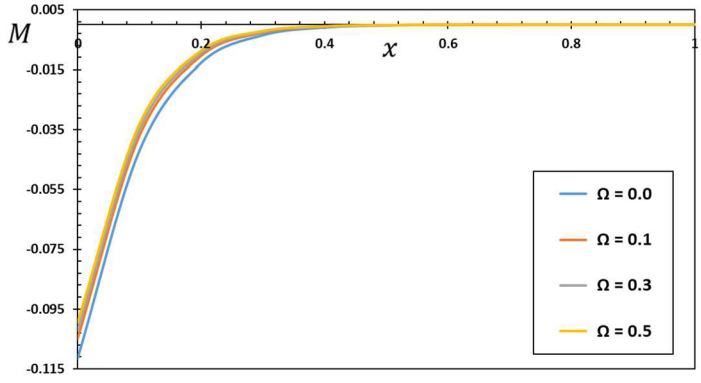


**Figure 5** The effect of rotation (Ω) on the variation of bending moment $M$

rise and reach their highest point at the first side of the beam as a result of the convective load that the beam is subjected to. Then, as $x$ increases toward the other end of the beam, the heat wave's ability to get there diminishes until it finally fades away. Changing the axial direction of the nanobeam lowers its temperature along its length. Contrary to the predictions made by the conventional theory of convection, heat waves travel through a medium

at a slower rate than would be consistent with physics. These observations are consistent with those obtained in the previous literature, including those found by the investigators in [50, 51].

In Fig. 4, we have a graphic made to examine the impact of the speed of rotation $\Omega$ on the change in the axial displacement $u$. We can see that the displacement $u$ is greatest at the initial end of the nanobeam, then reduces to its smallest at the point $x \cong 0.22$, and finally rises to its value of zero as we move to the opposite edge. We also found that mechanical waves travel in a restricted area. Finally, this graph displays that as the rotational speed rises, the absolute value of the deformations $u$ decreases.

As shown in Fig. 5, changing values of the angular velocity of rotation $\Omega$ cause the patterns of bending moment $M$ to change within the rotating nanobeam. Figure 5 displays that the bending moment $M$ is negative on the first side of the nanobeam and gradually increases until it disappears with time in the direction it reaches the other side of the nanobeam. Although the effect of the two rotors is weak on the moment $M$, its absolute value increases with the increase in the rotation speed $\Omega$.

Therefore, it can be concluded that the rotation field plays a significant role in nanobeams' mechanical, thermal, and vibration behavior and that this analysis aspect should be considered when developing NEMS and MEMS devices. Since rotation analysis is one of the main goals of the present work, the analysis presented in this study can be used to design better the blades of micro devices such as rotating microturbines [52]. Moreover, the previous considerations allow us to conclude the significant effect of rotation on the response of the studied fields. These observations are also consistent with those found in the previous literature [53, 54].

The theory of nonlocal elasticity is based on the atomic theory of lattice dynamics in addition to the concept of phonon scattering. In this theory, the spatial weight is determined by a one-dimensional nonlocal parameter known as the attenuation function. The value of this coefficient depends on the length of the internal property of the material divided by the length of its external property. Several previous studies have shown that the effects of size and thermal stresses have a profound influence on the dynamic properties of materials at the nanoscale, making them very different from their behavior in the case of materials at larger scales.

In the second part of the discussion, the impact of the nonlocal factor $\xi$ on the behavior of the studied physical variables will be considered. These changes are represented in the graphs shown in Figs. 6–9. It is noted that in the case when $\xi = 0$, the results are described in the case of the traditional local theory, which does not take into account the effect of the scale. In the situation of the nonlocal thermoelasticity theory, three different nonzero values are taken into account, and they are $\xi = 0.3$, 0.5, and 0.7. In the numerical calculations in this case, it will be assumed that the other effective constants are constants ($\Omega = 0.3$, $Ve = 10$ V, $Re = 300$, $\tau_q = 0.05$, and $\tau_\theta = 0.02$). According to the numerical data presented in the figures, it is seen that the nonlocal index $\xi$ has a great effect on the behavior of all the physical fields under consideration. From Figs. 6, 8, and 9, it is clear that the deflection $w$, displacement $u$, and moment $M$ are greatly influenced by the change of this parameter, while in Fig. 7, it is clear that it has a slight impact on the temperature $\theta$ and the propagation of the heat wave. The reason for this is due to the fact that the presence of the nonlocal index tends to decrease the stiffness of the nanobeams. The nonlocal parameter nondependence on temperature has been observed in many investigations and previous studies

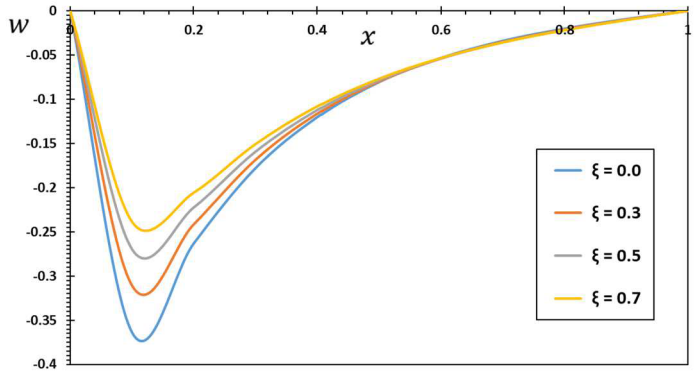


**Figure 6** The effect of nonlocality ($\xi$) on the variation of the deflection $w$

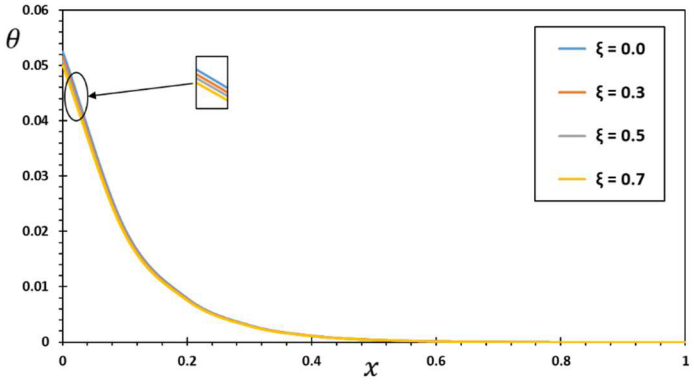


**Figure 7** The effect of nonlocality ($\xi$) on the variation of the temperature $\theta$

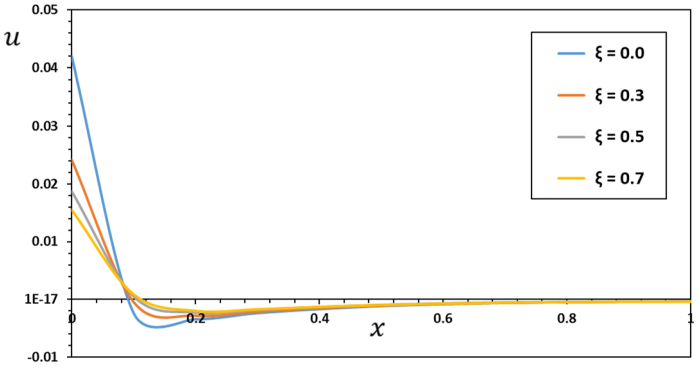


**Figure 8** The effect of nonlocality ($\xi$) on the variation of the displacement $u$

[55]. Other aspects for media with microstructure can be found in [56–61]. It can be concluded further that the steady state of the mechanical waves within the beam depends on specific values of the nonlocal index $\xi$.

Since the temperature of the conducting substances increases as the electric current flows through them, we say that it has a thermal impact. The magnitude of this tempera-

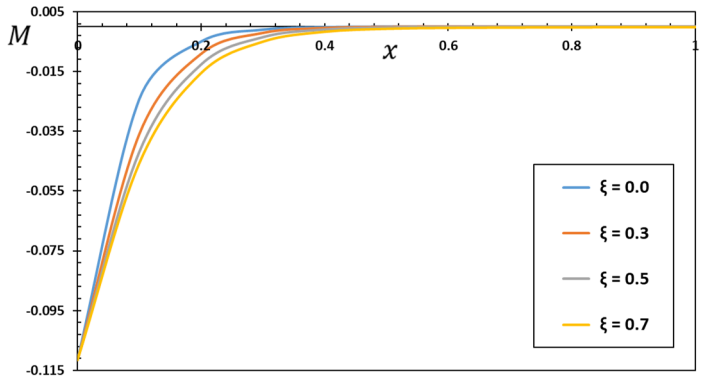


**Figure 9** The effect of nonlocality ($\xi$) on the variation of the bending moment $M$

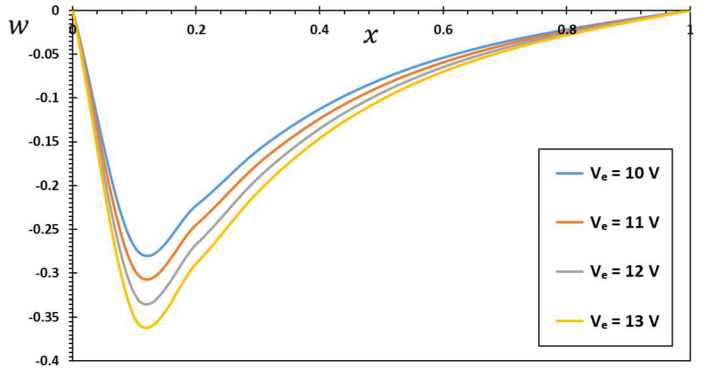


**Figure 10** The effect of electric voltage $V_e^2$ on the variation of the deflection $w$

ture's impact is determined by three primary factors: the resistance of the electrical conductor; the amount of time that the electric current flows through the conductor; and the magnitude of the electric current itself, which generates a larger amount of heat. The law of Joules provides a mathematical expression for this connection, stating that the amount of heat generated by an electric current is proportional to the square of the current multiplied by the length of time the current is passed through a specific conductor.

In the final part of the discussion, the numerical results of the studied domains will be presented in two sets of graphs. The first set of Figs. 10–13 displays the behavior of thermophysical domains such as thermal deflection $w$, displacement $u$, and temperature increase $\theta$ when the electrical resistance of a graphene strip is kept constant at 300 ohms and four different values of voltage $V_e$ are considered to be 10, 11, 12, and 13 volts. When the electrical resistance changes ($Re$ = 300, 350, 400, or 450 Ω) while the voltage remains constant at $V_e$ = 11 volts, the second group of Figs. 14–17 will be studied.

As can be shown in Figs. 10–13, an increase in electrical voltage $V_e$ results in an equivalent rise in all the investigated physical fields. The curves approach each other as one moves away from the electricity source, but their values fluctuate depending on the magnitude of the voltage $V_e$.

The resistance of conductive materials is expected to rise with the rise in temperature, while the resistance of insulating materials will decrease. In general, semiconductors have

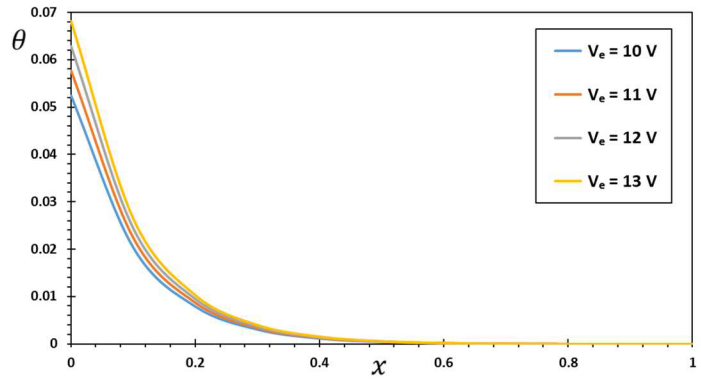


**Figure 11** The effect of electric voltage $V_e^2$ on the variation of the temperature $\theta$

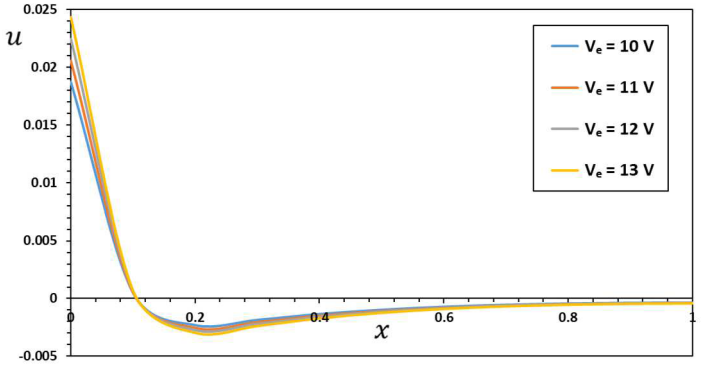


**Figure 12** The effect of electric voltage $V_e^2$ on the variation of the displacement $u$

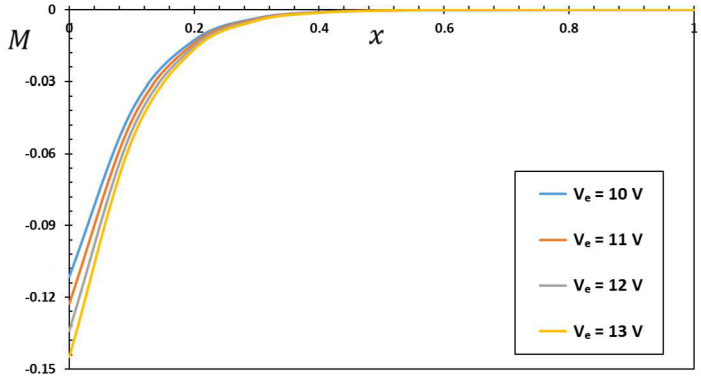


**Figure 13** The effect of electric voltage $V_e^2$ on the variation of the moment $M$

a lower resistance at higher temperatures. Figures 14 and 15 show that the value of the electrical resistance $Re$ has a significant influence on the height changes of the physical domains within the nanobeam, including temperature changes $\theta$ and deflection $w$. Also, one of the important conclusions that can be noted is that when the electrical resistance value increases, the value of the absolute value of these studied fields declines. It can also

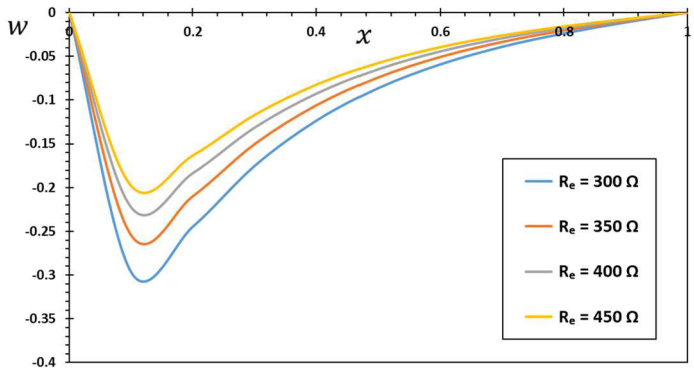


**Figure 14** The effect of electric resistance *Re* on the variation of deflection *w*

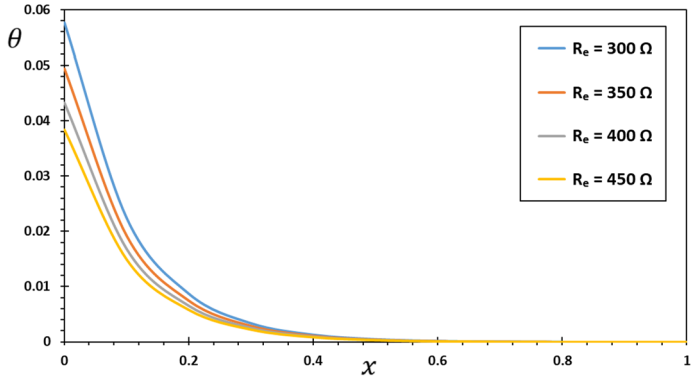


**Figure 15** The effect of electric resistance *Re* on the variation of temperature $\theta$

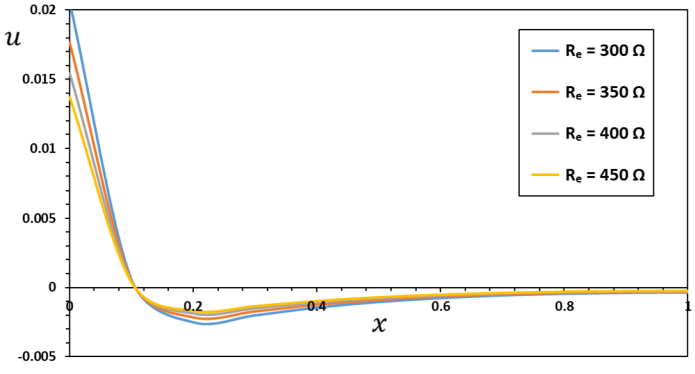


**Figure 16** The effect of electric resistance *Re* on the variation of displacement *u*

be noticed from graph 15 that the thermoelectric effect causes a rapid rise in temperature $\theta$ over a small distance near the first end of the beam, although the strength of the resulting curves varies with the electrical resistance *Re*. Three separate displacements *u* and bending moment *M* curves (Figs. 16 and 17) show how the peak values decrease with increasing electrical resistance values. It was found that the maximum values of these fields decreased with movement in the direction of the *x*-axis. Figure 17 presents the graphs of

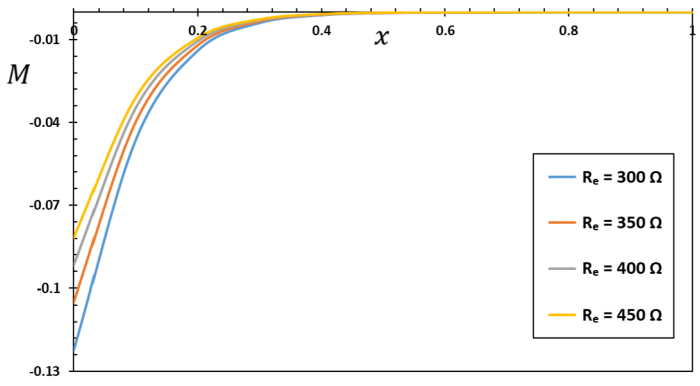


**Figure 17** The effect of electric resistance *Re* on the variation of bending moment *M*

the bending moment, which showed a single peak and a significant decrease in magnitude with increasing electrical resistance *Re*.

## 10 Conclusions

The current research proposes a revised nonlocal beam theory for investigating nanostructure systems that rotate along a fixed axis. In the formulations, the nonlocal constitutive relations discovered by Eringen as well as a modified thermoelastic framework with phase delays are utilized. After the governing system equations have been derived, the governing equations may be solved by applying the state-space technique as well as the Laplace transform methods. Nonlocality and beam rotation are also studied, and their implications on the topic under study are examined in depth.

When investigating nanostructures at the nanometer scale, it is common for nonlocal effects to become more noticeable. The results demonstrate that the nonlocal indicator has a small impact on how the nondimensional temperature changes but a big effect on how the nondimensional deflection, displacement, and bending moment peak values change. The angular velocity of rotation has a considerable influence on the distributions of different thermophysical domains except for temperature, where the effect is weak. From the results, it is seen that the magnitudes of these fields increase along with the rotational speed of the nanobeam around a fixed axis. The proposed model in this effort is able to investigate the thermal and mechanical vibrations of many structural systems, such as the beams and flaps of rotating nanopillars, in addition to the axial vibration of these beams. Also, the current work might contribute to a more in-depth comprehension of the dynamics of spinning nanobeams in some way.

## Appendix A

The coefficients $a_j$ after solving Eq. (57) can be written as

$$a_0(x,s) = -\frac{k_2^2k_3^2(k_2^2-k)\cosh(k_1x)+k_1^2k_3^2(k_3^2-k_1^2)\cosh(k_2x)+k_2^2k_1^2(k_1^2-k_2^2)\cosh(k_3x)}{(k_1^2-k_2^2)(k_2^2-k_3^2)(k_3^2-k_1^2)},$$

$$a_1(x,s) = -\frac{k_2^3k_3^3(k_2^2-k_3^2)\sinh(k_1x)+k_1^3k_3^3(k_3^2-k_1^2)\sinh(k_2x)+k_2^3k_1^3(k_1^2-k_2^2)\sinh(k_3x)}{k_1k_2k_3(k_1^2-k_2^2)(k_2^2-k_3^2)(k_3^2-k_1^2)},$$

$$a_2(x,s) = \frac{(k_2^4-k_3^4)\cosh(k_1x)+(k_3^4-k_1^4)\cosh(k_2x)+(k_1^4-k_2^4)\cosh(k_3x)}{(k_1^2-k_2^2)(k_2^2-k_3^2)(k_3^2-k_1^2)},$$

$$a_3(x,s) = \frac{k_2k_3(k_2^4-k_3^4)\sinh(k_1x) + k_1k_3(k_3^4-k_1^4)\sinh(k_2x) + k_1k_2(k_1^4-k_2^4)\sinh(k_3x)}{k_1k_2k_3(k_1^2-k_2^2)(k_2^2-k_3^2)(k_3^2-k_1^2)},$$

$$a_4(x,s) = \frac{(k_2^2-k_3^2)\cosh(k_1x) + (k_3^2-k_1^2)\cosh(k_2x) + (k_1^2-k_2^2)\cosh(k_3x)}{(k_1^2-k_2^2)(k_2^2-k_3^2)(k_3^2-k_1^2)},$$

$$a_5(x,s) = -\frac{k_2k_3(k_2^2-k_3^2)\sinh(k_1x) + k_1k_3(k_3^2-k_1^2)\sinh(k_2x) + k_1k_2(k_1^2-k_2^2)\sinh(k_3x)}{k_1k_2k_3(k_1^2-k_2^2)(k_2^2-k_3^2)(k_3^2-k_1^2)}.$$

## Appendix B

The elements $[L_{ij}(x,s)]$ of Eq. (58) can be expressed as follows:

$$L_{11}(x,s) = a_0 - a_4B_3, \qquad L_{12}(x,s) = -a_4B_4, \qquad L_{13}(x,s) = a_2 + a_4B_5,$$

$$L_{14}(x,s) = a_1 - a_5B_3, \qquad L_{15}(x,s) = -a_5B_4, \qquad L_{16}(x,s) = a_3 + a_5B_5,$$

$$L_{22}(x,s) = a_0 + a_2B_1 + a_4\left(B_1^2 + B_2B_4\right), \qquad L_{21}(x,s) = a_4B_2B_3,$$

$$L_{33}(x,s) = a_0 + a_2B_5 + a_4\left(B_2B_4 - B_3 + B_5^2\right), \qquad L_{23}(x,s) = -a_2B_2 - a_4B_2(B_1 + B_5),$$

$$L_{24}(x,s) = a_5B_2B_3, \qquad L_{35}(x,s) = -a_3B_4 - a_5B_4(B_1 + B_5),$$

$$L_{25}(x,s) = a_1 + a_3B_1 + a_5\left(B_1^2 + B_2B_4\right), \qquad L_{26}(x,s) = -a_3B_2 - a_5B_2(B_1 + B_5),$$

$$L_{31}(x,s) = -a_2B_3 - a_4B_5B_3, \qquad L_{32}(x,s) = -a_2B_4 - a_4B_4(B_1 + B_5),$$

$$L_{34}(x,s) = -a_3B_3 - a_5B_5B_3, \qquad L_{36}(x,s) = a_1 + a_3B_5 + a_5\left(B_2B_4 - B_3 + B_5^2\right),$$

$$L_{46}(x,s) = a_2 + a_4B_5, \qquad L_{45}(x,s) = -a_4B_4 \qquad L_{41}(x,s) = -a_3B_3 - a_5B_5B_3,$$

$$L_{42}(x,s) = -a_3B_4 - a_5B_4(B_1 + B_5), \qquad L_{44}(x,s) = a_0 - a_4B_3,$$

$$L_{43}(x,s) = a_1 + a_3B_5 + a_5\left(B_2B_4 - B_3 + B_5^2\right), \qquad L_{51}(x,s) = a_3B_2B_3 + a_5B_2B_3(B_1 + B_5),$$

$$L_{52}(x,s) = a_1B_1 + a_3\left(B_2B_4 + B_5^2\right) + a_5\left(B_1^3 + 2B_1B_2B_4 + B_2B_4B_5\right),$$

$$L_{53}(x,s) = -a_1B_2 - a_3B_2(B_1 + B_5) - a_5B_2\left(B_1B_5 + B_5^2 + B_1^2 - B_3 + B_2B_4\right),$$

$$L_{54}(x,s) = a_4B_2B_3, \qquad L_{55}(x,s) = a_0 + a_2B_1 + a_4\left(B_1^2 + B_4B_2\right),$$

$$L_{56}(x,s) = -a_2B_2 - a_4B_2(B_1 + B_5),$$

$$L_{61}(x,s) = -a_1B_3 - a_3B_3B_5 - a_5B_2\left(B_5^2 - B_3 + B_2B_4\right), \qquad L_{64}(x,s) = -a_2B_3 - a_4B_5B_3,$$

$$L_{62}(x,s) = -a_1B_4 - a_3B_4(B_1 + B_5) - a_5B_4\left(B_1B_5 + B_5^2 + B_1^2 - B_3 + B_2B_4\right),$$

$$L_{63}(x,s) = a_1B_5 + a_3\left(B_5^2 - B_3 + B_2B_4\right) + a_5\left(B_1B_2B_4 + 2B_4B_1B_5 + B_5^3 + B_1^2 - 2B_3B_5\right),$$

$$L_{65}(x,s) = -a_2B_4 + a_4(B_1 + B_5), \qquad L_{66}(x,s) = a_0 + a_2B_5 + a_4\left(B_5^2 - B_3 + B_4B_2\right).$$

**Acknowledgements**
The authors thank the King Saud University, Riyadh, Saudi Arabia, which funded this project.

**Funding**
This project is funded by the Research Supporting Project number (RSP2023R167), King Saud University, Riyadh, Saudi Arabia.

**Abbreviations**
$T_0$, Reference temperature; $(x, y, z)$, Cartesian coordinates; $u$, $v$, $w$, Displacements; $\sigma_{ij}$, Local stress tensor; $\varepsilon_{ij}$, Strain tensor; $\theta = T - T_0$, Change in temperature; $\rho$, Density; $k = K/\rho C_E$, Thermal diffusivity; $K$, Thermal conductivity; $\tau_{ij}$, Nonlocal stress tensor; $C_E$, Specific heat; $E$, Young's modulus; $\nu$, Poisson's ratio; $\alpha_t$, Coefficient of thermal expansion; $\delta_{ij}$, Kronecker delta function; $\gamma = \frac{\alpha_t E}{1-2\nu}$, Thermal coupling; $\lambda$, $\mu$, Elastic Lame's constants; $L$, Length; $b$, Width; $h$, Thickness; $w(x, t)$, Transversal deflection; $A = bh$, Cross-sectional area; $I = bh^3/12$, Moment of inertia,; $EI$, Flexural rigidity; $M_T$, Thermal moment; $Q$, Internal energy source; $\rho$, The density of the material.

**Availability of data and materials**
Not applicable.

## Declarations

**Ethics approval and consent to participate**
Not applicable.

**Competing interests**
The authors declare no competing interests.

**Author contributions**
A.E.A. coordinated the manuscript; M.M. performed all the mathematical calculations; S.S.A. prepared the graphics. All three authors supervised the entire manuscript and agreed with this final form of the manuscript.

**Author details**
[1]Department of Mathematics, Faculty of Science, Mansoura University, Mansoura 35516, Egypt. [2]Department of Mathematics and Computer Science, Transilvania University of Brasov, Brasov, Romania. [3]Department of Statistics and Operations Research, College of Science, King Saud University, P.O. Box 2455, Riyadh 11451, Saudi Arabia.

## Publisher's Note


Received: 8 February 2023 Accepted: 23 February 2023 Published online: 06 March 2023

**References**
1. Malik, M., Das, D.: Free vibration analysis of rotating nano-beams for flap-wise, chord-wise and axial modes based on Eringen's nonlocal theory. Int. J. Mech. Sci. **179**, 105655 (2020)
2. Kim, K., Xu, X., Guo, J., Fan, D.L.: Ultrahigh-speed rotating nanoelectromechanical system devices assembled from nanoscale building blocks. Nat. Commun. **5**, 3632 (2014)
3. Li, J., Wang, X., Zhao, L., Gao, X., Zhao, Y., Zhou, R.: Rotation motion of designed nano-turbine. Sci. Rep. **4**(1), 5846 (2014)
4. Khaniki, H.B.: Vibration analysis of rotating nanobeam systems using Eringen's two-phase local/nonlocal model. Physica E, Low-Dimens. Syst. Nanostruct. **99**, 310–319 (2018)
5. Ganguli, R., Panchore, V.: The Rotating Beam Problem in Helicopter Dynamics. Foundations of Engineering Mechanics. Springer, Berlin (2018)
6. Yao, M.H., Chen, Y.P., Zhang, W.: Nonlinear vibrations of blade with varying rotating speed. Nonlinear Dyn. **68**(4), 487–504 (2012)
7. Ebrahimi, F., Barati, M.R., Haghi, P.: Wave propagation analysis of size-dependent rotating inhomogeneous nanobeams based on nonlocal elasticity theory. J. Vib. Control **24**(17), 3809–3818 (2018)
8. Narendar, S., Gopalakrishnan, S.: Nonlocal wave propagation in rotating nanotube. Results Phys. **1**, 17–25 (2011)
9. Hoshina, M., Yokoshi, N., Ishihara, H.: Nanoscale rotational optical manipulation. Opt. Express **28**, 14980–14994 (2020)
10. Nan, F., Li, X., Zhang, S., Ng, J., Yan, Z.: Creating stable trapping force and switchable optical torque with tunable phase of light. Sci. Adv. **8**, 46 (2022)
11. Abouelregal, A.E., Mohammad-Sedighi, H., Faghidian, S.A., Shirazi, A.H.: Temperature-dependent physical characteristics of the rotating nonlocal nanobeams subject to a varying heat source and a dynamic load. Facta Univ. Ser.: Mech. Eng. **19**(4), 633–656 (2021)
12. Narendar, S.: Mathematical modelling of rotating single-walled carbon nanotubes used in nanoscale rotational actuators. Def. Sci. J. **61**(4), 317–324 (2011)
13. Rahmani, A., Faroughi, S., Friswell, M.I.: The vibration of two-dimensional imperfect functionally graded (2D-FG) porous rotating nanobeams based on general nonlocal theory. Mech. Syst. Signal Process. **144**, 106854 (2020)
14. Tho, N.C., Thanh, N.T., Tho, T.D., Van Minh, P., Hoa, L.K.: Modelling of the flexoelectric effect on rotating nanobeams with geometrical imperfection. J. Braz. Soc. Mech. Sci. Eng. **43**(11), 510 (2021)
15. Mindlin, R., Tiersten, H.: Effects of couple-stresses in linear elasticity. Arch. Ration. Mech. Anal. **11**, 415–448 (1962)
16. Yang, F., Chong, A.C.M., Lam, D.C.C., Tong, P.: Couple stress based strain gradient theory for elasticity. Int. J. Solids Struct. **39**(10), 2731–2743 (2002)
17. Lam, D.C.C., Yang, F., Chong, A.C.M., Wang, J., Tong, P.: Experiments and theory in strain gradient elasticity. J. Mech. Phys. Solids **51**(8), 1477–1508 (2003)
18. Fan, F., Xu, Y., Sahmani, S., Safaei, B.: Modified couple stress-based geometrically nonlinear oscillations of porous functionally graded microplates using NURBS-based isogeometric approach. Comput. Methods Appl. Mech. Eng. **372**, 113400 (2020)
19. Eringen, A.C.: Non-local Continuum Field Theories, pp. 71–176. Springer, Berlin (2002)

20. Eringen, A.C.: Linear theory of nonlocal elasticity and dispersion of plane waves. Int. J. Eng. Sci. **10**(5), 425–435 (1972)
21. Eringen, A.C.: On differential equations of nonlocal elasticity and solutions of screw dislocation and surface waves. J. Appl. Phys. **54**(9), 4703–4710 (1983)
22. Jha, B.K., Oyelade, I.O.: The role of dual-phase-lag (DPL) heat conduction model on transient free convection flow in a vertical channel. Partial Differ. Equ. Appl. Math. **5**, 100266 (2022)
23. Cattaneo, C.: A form of heat conduction equation which eliminates the paradox of instantaneous propagation. C. R. Acad. Sci. **247**, 431–433 (1958)
24. Vernotte, P.: Paradox in the continuous theory of heat equation. C. R. Acad. Sci. **246**, 3154–3155 (1958)
25. Lord, H.W., Shulman, Y.: A generalized dynamical theory of thermoelasticity. J. Mech. Phys. Solids **15**(5), 299–309 (1967)
26. Green, A.E., Lindsay, K.A.: Thermoelasticity. J. Elast. **2**(1), 1–7 (1972)
27. Green, A.E., Naghdi, P.M.: On undamped heat waves in an elastic solid. J. Therm. Stresses **15**(2), 253–264 (1992)
28. Green, A.E., Naghdi, P.M.: Thermoelasticity without energy dissipation. J. Elast. **31**(3), 189–208 (1993)
29. Tzou, D.Y.: A unified field approach for heat conduction from macro-to micro-scales. J. Heat Transf. **117**(1), 8–16 (1995)
30. Tzou, D.Y.: The generalized lagging response in small-scale and high-rate heating. Int. J. Heat Mass Transf. **38**(17), 3231–3240 (1995)
31. Tzou, D.Y.: Experimental support for the lagging behavior in heat propagation. J. Thermophys. Heat Transf. **9**(4), 686–693 (1995)
32. Kraus, J.: Electromagnetics. McGraw-Hill, New York (1984)
33. Wang, H., Dong, K., Men, F., Yan, Y.J., Wang, X.: Influences of longitudinal magnetic field on wave propagation in carbon nanotubes embedded in elastic matrix. Appl. Math. Model. **34**(4), 878–889 (2010)
34. Narendar, S., Gupta, S.S., Gopalakrishnan, S.: Wave propagation in single-walled carbon nanotube under longitudinal magnetic field using nonlocal Euler–Bernoulli beam theory. Appl. Math. Model. **36**(9), 4529–4538 (2012)
35. Pradhan, S.C., Murmu, T.: Application of nonlocal elasticity and DQM in the flapwise bending vibration of a rotating nanocantilever. Physica E, Low-Dimens. Syst. Nanostruct. **42**(7), 1944–1949 (2010)
36. Babaei, A., Yang, C.X.: Vibration analysis of rotating rods based on the nonlocal elasticity theory and coupled displacement field. Microsyst. Technol. **25**, 1077–1085 (2019)
37. Abouelregal, A.E., Mohammed, F.A., Benhamed, M., Zakria, A., Ahmed, I.-E.: Vibrations of axially excited rotating micro-beams heated by a high-intensity laser in light of a thermo-elastic model including the memory-dependent derivative. Math. Comput. Simul. **199**, 81–99 (2022)
38. Abouelregal, A.E., Alesemi, M.: Fractional Moore–Gibson–Thompson heat transfer model with nonlocal and nonsingular kernels of a rotating viscoelastic annular cylinder with changeable thermal properties. PLoS ONE **17**(6), e0269862 (2022)
39. Sosa, H.A., Bahar, L.Y.: The state space approach to thermoelasticity: a reformulation and an alternate approach. J. Therm. Stresses **16**(4), 421–436 (1993)
40. Abd El-Latief, A.M.: New state-space approach and its application in thermoelasticity. J. Therm. Stresses **40**(2), 135–144 (2016)
41. Bahar, L.Y., Hetnarski, R.B.: State space approach to thermoelasticity. J. Therm. Stresses **1**(1), 135–145 (1978)
42. Sherief, H.H.: State space approach to thermoelasticity with two relaxation times. Int. J. Eng. Sci. **31**(8), 1177–1189 (1993)
43. Alahmadi, A.N.M.: Vibration of a thermoelastic microbeam due to the thermoelectrical effect of a strip of graphene. Math. Probl. Eng. **2022**, 4935623 (2022)
44. Voršič, Ž., Maruša, R., Pihler, J.: New method for calculating the heating of the conductor. Energies **12**(14), 2769 (2019)
45. Abate, J.: Numerical inversion of Laplace transforms of probability distributions. ORSA J. Comput. **7**, 36–43 (1995)
46. Crump, K.S.: Numerical inversion of Laplace transforms using a Fourier series approximation. J. ACM **23**, 89–96 (1976)
47. Luschi, L., Pieri, F.: An analytical model for the determination of resonance frequencies of perforated beams. J. Micromech. Microeng. **24**(5), 055004 (2014)
48. Sudak, L.J.: Column buckling of multiwalled carbon nanotubes using nonlocal continuum mechanics. J. Appl. Phys. **94**(11), 7281–7287 (2003)
49. Abouelregal, A.E., Tiwari, R.: The thermoelastic vibration of nano-sized rotating beams with variable thermal properties under axial load via memory-dependent heat conduction. Meccanica **57**, 2001–2025 (2022)
50. Abouelregal, A.E., Khalil, K.M., Mohammed, W.W., Atta, D.: Thermal vibration in rotating nanobeams with temperature-dependent due to exposure to laser irradiation. AIMS Math. **7**(4), 6128–6152 (2022)
51. Jahangir, A., Ali, H., Mahmood, A., Zaigham Zia, Q.M.: Study on reflected waves through visco-elastic solid rotating with fixed angular frequency. Waves Random Complex Media (2023). https://doi.org/10.1080/17455030.2023.2171503
52. Fang, J., Yin, B., Zhang, X., Yang, B.: Size-dependent vibration of functionally graded rotating nanobeams with different boundary conditions based on nonlocal elasticity theory. Proc. Inst. Mech. Eng., Part C, J. Mech. Eng. Sci. **236**(6), 2756–2774 (2022)
53. Atta, D., Abouelregal, A.E., Alsharari, F.: Thermoelastic analysis of functionally graded nanobeams via fractional heat transfer model with nonlocal kernels. Mathematics **10**, 4718 (2022)
54. Yan, X.: Free vibration analysis of a rotating nanobeam using integral form of Eringen's nonlocal theory and element-free Galerkin method. Appl. Phys. A **128**, 641 (2022)
55. Jin-Tao, M., Tian-Hu, H.: Investigation on the dynamic responses of a generalized thermoelastic problem with variable properties and nonlocal effect. J. Therm. Stresses **42**(4), 426–439 (2019)
56. Abouelregal, A.E., Marin, M.: The response of nanobeams with temperature-dependent properties using state-space method via modified couple stress theory. Symmetry **12**(8), Art. No. 1276 (2020)
57. Scutaru, M.L., Vlase, S., et al.: New analytical method based on dynamic response of planar mechanical elastic systems. Bound. Value Probl. **2020**(1), Art. No. 104 (2020)
58. Marin, M., Ellahi, R., et al.: On the decay of exponential type for the solutions in a dipolar elastic body. J. Taibah Univ. Sci. **14**(1), 534–540 (2020)
59. Abo-Dahab, S.M., et al.: Generalized thermoelastic functionally graded on a thin slim strip non-Gaussian laser beam. Symmetry **12**(7), Art. No. 1094 (2020)

60. Alzahrani, F., Hobiny, A., et al.: An eigenvalues approach for a two-dimensional porous medium based upon weak, normal and strong thermal conductivities. Symmetry **12**(5), Art. No. 848 (2020)
61. Rachid, K., Bourouina, H., Yahiaoui, R., Bounekhla, M.: Magnetic field effect on nonlocal resonance frequencies of nanobeam with periodic square holes network. Physica E, Low-Dimens. Syst. Nanostruct. **105**, 83–89 (2019)